# Improving the PAD actuator performances by vector control

Christophe Giraud-Audine, *Member, IEEE,* Frédéric Giraud, *Member, IEEE,* Michel Amberg, Charles Mangeot, and Betty Lemaire-Semail, *Member, IEEE*

*Abstract*—In this work, we address the problem of pull-out and stalling of the vector control of the piezo-actuator drive (PAD). The model presented reveals the similarities with synchronous machine and therefore we propose the vector control to solve the problem and to enhance its performances. The implementation using a position sensor is tested. Experimental results show that the vector control avoids pull-out and reduces dramatically the voltage applied to achieve the same performances. Speed up to 2.5 times the maximum rated speed at full load could be achieved without loss of synchronization.

*Index Terms*—piezoelectric actuators, servomotors, motion control, machine vector control, magnetic compatibility, magnetic resonance imaging

## I. INTRODUCTION

Robotically assisted surgical interventions provide precision, speed and offer possibility for remote operation. MRI guidance, by periodically providing accurate images, helps to update the trajectory of surgical instruments. However, such applications face harsh space constraints, and to preserve the image quality, they should operate without distorting the magnetic field [1]. This has direct impact on the materials used, and the actuator technology. Conventional electromagnetic actuators must therefore be left outside the MRI bore, which results in complex kinematics to control the tools [2]. Research have therefore also focused on other actuation principles such as hydraulic [3], pneumatic [4]–[8] or piezoelectric actuators [9], [10]. Pneumatic actuators are MR compatible. However, the distribution circuit is bulky and must be deported outside the MRI hole. Due to the compressibility of gas and the long circuits, non-linearity can lead to a complex control [4], [11]. Hydraulic actuation [3] does not have this drawback, however leakage can be an issue. Piezoelectric actuators have often been used [6], [9], [10], [12], [13], although according to some authors, they have a negative impact on the signal to noise ratio so interleaved operation between imaging and actuation or careful selection of the scanning parameters is recommended [14], [15]. This problem results from the high voltages at high frequency that must be applied to the actuators and can be attenuated by a cautious design of the power supply [9]. Piezoelectric actuator drive (PAD) motors are low speed, high

C. Giraud-Audine, F. Giraud, M. Amberg and B. Lemaire-Semail are with the Laboratoire d'Electrotechnique et d'Electronique de Puissance - L2EP - EA 2697, Univ. Lille, Centrale Lille, Arts et Métiers ParisTech, HEI, HeSam, , F-59000 Lille, France (e-mail: christophe.giraud-audine@ensam.eu).

C. Mangeot is with NOLIAC a part of CTS corporation, Hejreskovvej 18,3490 Kvistgaard, Denmark.

precision piezoelectric motors working on a conversion principle that does not rely on resonance (as opposed to ultrasonic motors), hence the frequency of the driving signals is much lower [16]. Recently, NOLIAC proposed a new low power design in non-magnetic materials suitable for use in RMI. So far the speed is limited due to pull-out where the gearing may disengage causing temporary loss of synchronicity, and therefore compromising the natural positioning capability of the motor. This can even cause stalling of the motor. In many user case, precise positioning and high speed operations are required, and this limitation is severe. In fact, the PAD motor can run at higher speed, although some anomalies were observed in the vicinity of resonance [17]. In [18], a simplified model of the PAD dynamics including the contact provided some insight of the phenomena affecting the contact forces and the torque, and it was experimentally verified that the pull-off occurred at significantly higher frequencies if the nominal voltage was used. However, the reactive current can be prohibitive. So, in order to use the desirable features offered by this technology, there is a need to overcome the pull-out/stalling of the motor and to keep the voltages amplitude as low as possible.

This paper proposes to transpose the principle of vector control and experimentally demonstrates the enhancement over open loop operation. In the first part, by contrast with [19], the dynamic model is described in a particular rotating frame which naturally leads to a control structure similar to vector control. Basically, controlling in the rotating frame is equivalent to control the voltage phase relative to the mechanical angle yielding robustness with regards to pull-out. Based on this result the control structure is proposed in the second part. The third part deals with experimental validation. A very simple control is implemented in order to highlight the benefit of the strategy. Pull out is effectively handled, even in the case of non-linearities and saturation of the controller. The last part is devoted to discussion and conclusion.

## II. MODEL OF THE PIEZOELECTRIC DRIVE

### A. Principle

The PAD motor features two sets of piezoelectric actuators acting along two perpendicular directions as depicted on fig. 1. They are supplied with two sinusoidal voltages in quadrature, denoted $V_x$ and $V_y$, which results in a circular translation of the crown wheel. When brought into contact with the geared shaft, this wobbling movement is converted into a rotation of the shaft. The micro-toothed gear adds a high gear ratio thus
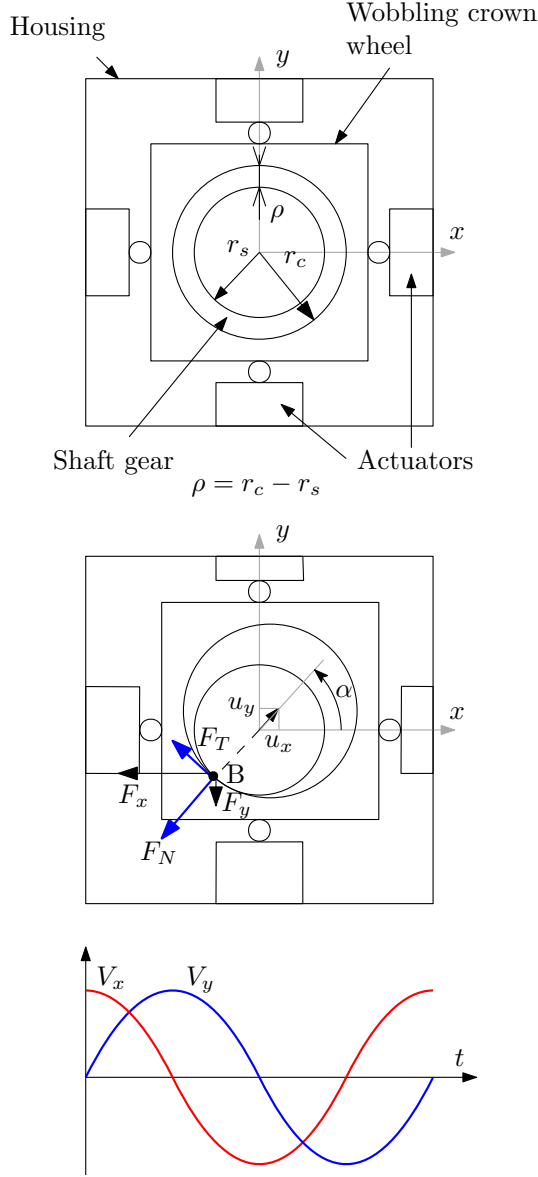
Fig. 1. Architecture of the PAD at rest (left) and during operation (middle) when supplied with two phase sinusoidal voltage (bottom)

allowing ultra low speed operation and exceptional positioning capabilities. There is therefore a direct relationship between the elongation of the actuators and the rotation angle of the shaft.

As for the piezoelectric actuators, the voltages $V_x$ and $V_y$ create stress in the material. This results in a deformation which is limited by the material's stiffness that tends to restore the initial shape of the actuators. Therefore, based on the inverse piezoelectric effect, a linear model of the forces applied to the crown wheel by the actuators is:

$$\mathbf{F}_a = \begin{pmatrix} F_x \\ F_y \end{pmatrix} = 2 \begin{pmatrix} NV_x - K_s u_x \\ NV_y - K_s u_y \end{pmatrix} \quad (1)$$

where $u_x$ and $u_y$ denote the displacement of the crown wheel in the the x and y directions respectively, $K_s$ is the elasticity of the actuator, and $N$ denotes the electromechanical

ratio. The linear model is of course a simplification of the actual piezo actuators behaviour and does not include creep and hysteresis since the crown wheel displacement can be reasonably considered negligible compared to the no-load displacement of the actuators.

It follows from the equation 1 that the voltages will control the forces generated at the contact. These forces are critical to control the motor, and the dynamic model derived in the next part will be used to propose a new control strategy.

### B. Dynamic model

In the sequel, in order to elaborate a general strategy, the following assumptions are made to capture the essential principle of the motor :

- the path of the motion is circular, i.e physical shape errors of the microgear are neglected,
- the path is concentric with the motion of the piezo actuators, in other words, the motor is perfectly centered,
- contact of the gearing is always maintained.

We consider the Lagrange equations. The kinematic constraints are included by introducing lagrange multipliers, which represent the forces resulting from these constraints. For that purpose, the crown wheel displacement vector $\mathbf{u} = (u_x, u_y)^T$ is given in its general form:

$$\mathbf{u} = \begin{pmatrix} u_x \\ u_y \end{pmatrix} = \begin{pmatrix} r \cos \alpha \\ r \sin \alpha \end{pmatrix} \quad (2)$$

where $r$ is the module of the displacement vector, and $\alpha$ its argument. The voltages are chosen as the electrical generalized coordinates of the model. The lagrangians for the actuators and the moving parts of the motor are then :

$$
\begin{aligned}
\mathcal{L}_x &= \tfrac{1}{2} M \left( -r\dot{\alpha} \sin \alpha + \dot{r} \cos \alpha \right)^2 - \\
&\quad - \left( \tfrac{1}{2} K_s u_x^2 - N V_x r \cos \alpha - \tfrac{1}{2} C V_x^2 \right) \\
\mathcal{L}_y &= \tfrac{1}{2} M \left( r\dot{\alpha} \cos \alpha + \dot{r} \sin \alpha \right)^2 - \\
&\quad - \left( \tfrac{1}{2} K_s u_y^2 - N V_y r \sin \alpha - \tfrac{1}{2} C V_y^2 \right) \\
\mathcal{L}_r &= \tfrac{1}{2} J_r \dot{\theta}^2 \\
\mathcal{L}_s &= \tfrac{1}{2} M_s \left( \left( -r\dot{\alpha} \sin \alpha + \dot{r} \cos \alpha \right)^2 + \right. \\
&\quad \left. + \left( r\dot{\alpha} \cos \alpha + \dot{r} \sin \alpha \right)^2 \right)
\end{aligned}
\quad (3)
$$

with $M, M_s$ the inertia of the actuators and the wobbling crown respectively, $J_r$ the rotation inertia of the shaft and gear, and $C$ the blocked capacitance of the actuators. The lagrangian associated to the motor is formed by adding the above lagrangians $\mathcal{L} = \mathcal{L}_x + \mathcal{L}_y + \mathcal{L}_s + \mathcal{L}_r$.

The kinematic constraint induced by the crowning/gear contact and the gearing are :

$$r - \rho = 0 \quad \text{and} \quad \theta - k\alpha = 0 \quad (4)$$

where $\theta$ is the angular position of the motor shaft and $k$ is the reduction ratio of the gearing. Since $F_N$ and $T_c$, respectively the force and torque involved to realize these constraints produce no work, one has $\mathcal{W}_c = (r - \rho)F_N + (\theta - k\alpha)T_c = 0$.

To account for the losses in the actuator, a Rayleigh potential is also added :

$$\mathcal{W}_{diss} = \frac{1}{2}d\left((-r\dot\alpha\sin\alpha + \dot r\cos\alpha)^2 \right.$$
$$\left. + (r\dot\alpha\cos\alpha + \dot r\sin\alpha)^2\right) \quad (5)$$

where $d$ denotes the linear damping coefficient. Finally, denoting $T$ the torque applied to the shaft, and $Q_x$, $Q_y$ the charges supplied by the generators, the work of the external force is $W_{ext} = T\theta - Q_xV_x - Q_yV_y$. The Lagrange procedure yields the equations by calculating $\frac{d}{dt}\frac{\partial\mathcal{L}}{\partial\dot q} - \frac{\partial\mathcal{L}}{\partial q} = \frac{\partial(\mathcal{W}_{ext}+\mathcal{W}_c)}{\partial q} - \frac{\partial\mathcal{W}_{diss}}{\partial\dot q}$, with the generalized displacements $q = \{r, \alpha, \theta, V_x, V_y\}$. Thus, the mechanical equations are :

$$F_N = M_T\rho k^2\Omega^2 - K_s\rho + N\left(V_x\cos k\theta + V_y\sin k\theta\right) \quad (6a)$$

$$J_{eq}\dot\Omega + kd\rho^2\Omega = \frac{N\rho}{k}\left(-V_x\sin k\theta + V_y\cos k\theta\right) + T \quad (6b)$$

with $M_T = M + M_s$, $J_{eq} = \frac{M_T\rho^2}{k^2} + J_r$ the equivalent moment of inertia, and $\Omega = \dot\theta$
The electric charges are :

$$Q_x = N\rho\cos k\theta + CV_x \quad (7a)$$
$$Q_y = N\rho\sin k\theta + CV_y \quad (7b)$$

## III. CONTROL IN THE ROTATING FRAME

### A. Electromechanical torque

The model gives some insight on how the torque is produced. Considering eq. (6b) one can recognize the electromechanical torque as :

$$T_m = \frac{N\rho}{k}\left(-V_x\sin\alpha + V_y\cos\alpha\right) \quad (8)$$

Define the "electrical" force vector $\mathbf{F} = (NV_x, NV_y)^T$, one can recognize that :

$$T_m = \frac{1}{k}\mathbf{u}\wedge\mathbf{F} \quad (9)$$

So in order to ensure a constant torque it follows that the two vectors should be synchronous. To do so the supply phase is directly controlled by the shaft position as follows :

$$\begin{cases} V_x = V\cos\left(k\theta + \phi\right) \\ V_y = V\sin\left(k\theta + \phi\right) \end{cases} \quad (10)$$

provided that the shaft angular position $\theta$ is measured. $\phi$, the phase of the voltages at $\theta = 0$, and $V$ are then the control variables of the torque as applying the constraint (10) and the kinematic constraint imposed by the gearing into the torque expression gives :

$$\begin{cases} T_m = NV\rho\left(-\cos\left(k\theta + \phi\right)\sin k\theta + \sin\left(k\theta + \phi\right)\cos k\theta\right) \\ \alpha = k\theta \end{cases}$$

$$\Rightarrow T_m = N\rho V\sin\left(\phi\right) \quad (11)$$

which confirms the observations discussed above.
On the other hand, there is an additional constraint, which is that the contact between the gearing elements must be
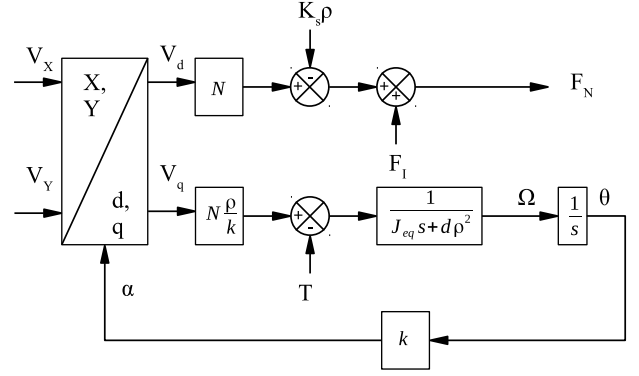


Fig. 2. Bloc diagram of the model in the $\{d, q\}$ frame

maintained. The contact force is given by the eq. (6a) which features three contributions:

- the centrifugal force : $F_I = M_T\rho k^2\Omega^2$ ;
- the adverse force due to the elasticity of the actuators: it is constant when the contact is established, but requires a minimum voltage before operation can actually occur;
- the voltage controlled contact force, which is given by the projection of $\mathbf{F}$ on the unit vector in the direction of $\mathbf{u}$ : $(V_x\cos\alpha + V_y\sin\alpha) = \frac{\mathbf{u}}{\|\mathbf{u}\|}\cdot\mathbf{F} = \mathbf{n}\cdot\mathbf{F}$

where $\mathbf{n}$ is the unit vector with direction $\mathbf{u}$. Therefore, unlike electromagnetic machines where the current can be fully employed to generate the torque, some of the voltage is necessary only to maintain the contact. The following subsection proposes a decoupled model in a rotating frame that simplifies the control.

### B. Model in the rotating frame and strategy

Since the voltages will be modulated according to eq. (10), and following the classic transformation used for electromagnetic drives, a frame rotating according to the electric angle $\alpha = k\theta$ is used. Hence, considering a vector $\mathbf{z}$ expressed in the reference frame $\mathbf{z} = (z_x, z_y)^T$ and the same vector expressed in the rotating frame $\mathbf{z} = (z_d, z_q)^T$, the rotational mapping is:

$$\begin{pmatrix} z_x \\ z_y \end{pmatrix} = \begin{pmatrix} \cos\alpha & \sin\alpha \\ -\sin\alpha & \cos\alpha \end{pmatrix}\begin{pmatrix} z_d \\ z_q \end{pmatrix} \quad (12)$$

and, thus eq (6a) and (6b) are rewritten as:

$$F_N = \left(M + M_s\right)\rho k^2\Omega^2 - K_s\rho + NV_d \quad (13a)$$
$$J_{eq}\dot\Omega + kd\rho^2\Omega = N\rho V_q + kT \quad (13b)$$

The model in the new rotating frame epicted on fig. 2 is now decoupled, allowing a simplified control scheme to be implemented. It can be observed that now the torque $T_m$ is controlled by the voltage $V_q$, and $V_d$ may be used to adjust the normal force. Hence, if the motor is directly controlled in the $\{d, q\}$ frame, it suffices to set a controller that generates the $V_q$ reference to follow a speed reference. $V_d$ is used to ensure the contact and should be minimal in order to limit the applied voltage. Then, by measuring the shaft position, it is possible to calculate $\alpha$ and then generate the actual voltages $V_x$ and $V_y$ according to eq. 12.
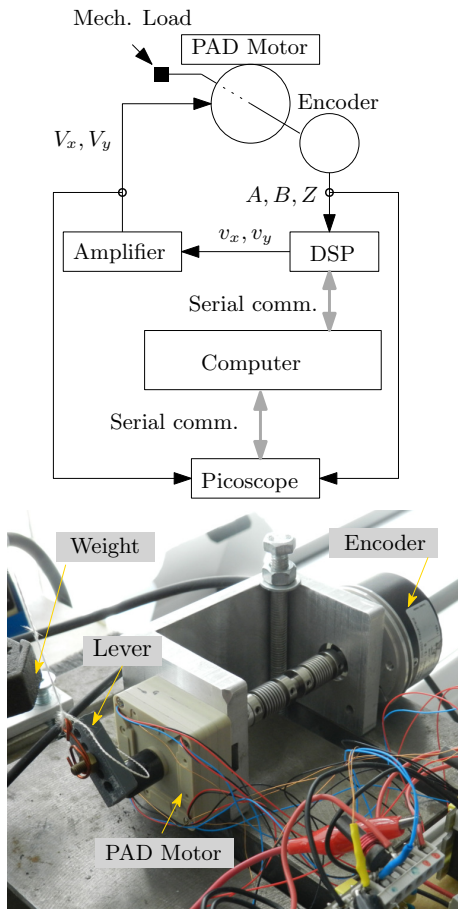
Fig. 3. Schematic and picture of the experimental rig.

As a final remark to this part, it can also be deduced from eq. (7a) and (7b) that the actual position of the wobbling crown can be deduced from measurement of the charges $Q_x$ and $Q_y$ as devised in [19]. In this work, however, the phase of the voltage were controlled thanks to a phase lock loop, but there was no control of their amplitudes. Besides, this strategy requires a good knowledge of the capacitance of the actuator which may vary with external factors such as temperature, and charge measurements are susceptible to drift due to the integration of quiescent currents of the operational amplifiers.

## IV. EXPERIMENTAL VALIDATION

### A. Experimental setup

For this investigation the motor considered is a PAD 7344 manufactured by Noliac (NOLIAC CTS, Kvistgaard, DK) ) a low power actuator designed for non-magnetic applications such as MRI scanners. The actuator main specifications are $15\,\mathrm{mN\,m}$ , maximum speed $67\,\mathrm{rev\,min^{-1}}$ and recommended speed $16.8\,\mathrm{rev\,min^{-1}}$ for continuous operation. The prime movers are multilayers piezoelectric benders and the motor is realized in non magnetic materials. The benders are very compact and the form factor of the actuator consisting in the assembly of four benders is low ($42 \times 42 \times 21\,\mathrm{mm^3}$, weight: $41\,\mathrm{g}$). On the other hand, the forces developed are small, and due to the low rigidity of the benders, the actuator is prone to

disengagement of the gearing at high speed.

A picture of the set-up used in this study is presented on fig. 3. The actuator is fixed on a plate and connected to an incremental rotary encoder (Baumer 16.05A10000-12-5, Frauenfeld, CH) by sleeves coupling to avoid to apply parasitic torques due to misalignment. The sensor is connected to an eZdsp TMS320F25 DSP board to compute the voltage references $V_d$ and $V_q$, and to perform the $\{d, q\} \rightarrow \{x, y\}$ transformation thanks to the measured shaft angle. These voltages are then amplified by two analog amplifiers (NF Corp. HSA4052, Yokohama, JP) to yield voltages that are limited to $100\,\mathrm{V_{pk\text{-}pk}}$. The closed loop sampling time is $4\,\mathrm{kHz}$. Data are acquired using picoscopes synchronized with the zero top of the encoder.

The mechanical load is realized by attaching a weight to a lever attached to the shaft. Therefore it is non-linear and adds inertia in the system.

### B. Open-loop performances

The PAD 7344 used in this study has a very low inertia. It is therefore very sensitive to imperfections. Fig. 4-a shows two tests in open loop : a constant voltage of $100\,\mathrm{V}$ is set, then once the contact between the wobbling crown and the shaft gear is established, the frequency of the alternative voltages were set, first to $20\,\mathrm{Hz}$, then to $100\,\mathrm{Hz}$. The mechanical position is calculated using the encoder signals. The response is fast and the gearing profile can be observed from the periodic speed variation superimposed to the transient response. To confirm this, The graph 4-b depicts mechanical instantaneous speed vs position: the periodicity is indeed the same on both curve, and is equal to the electric period. By design, the position is imposed by the gearing so any eccentricity or variation in the teeth shape also reflects in the speed.

Actually, as described by the model, the dynamic between the voltage and the speed is only due to inertia and damping of the actuator. The actuators frequency responses were measured after disassembling the rotor. Resonances occurred at $720\,\mathrm{Hz}$ and $740\,\mathrm{Hz}$ for the x and y axis respectively. So as a first approximation the transfer function of the speed vs voltage is established by neglecting the acceleration in eq (6b), and it melts down to a simple gain [19]. This is a valid approximation given that the desired dynamic in close loop does not exceed the actual cut-off frequency of the actuator. To demonstrate the benefit of the control in the rotating frame to handle pull-out, a basic control is implemented. An integral controller is implemented in order to control the speed near the reference without trying to compensate for the speed variation induced by the gearing. At frequencies beneath resonance, the closed loop dynamic is equivalent to a first order with unit gain. the time response is fixed by the choice of the integral gain. Note that, as the system is a first order, the closed loop is stable as long as the contact remains that is no pull out occurs. Thus, the experimental focus on the assessment of pull-out mitigation and control performances is out of the scope of the paper. The schematic of the closed loop control is depicted on Fig 5.
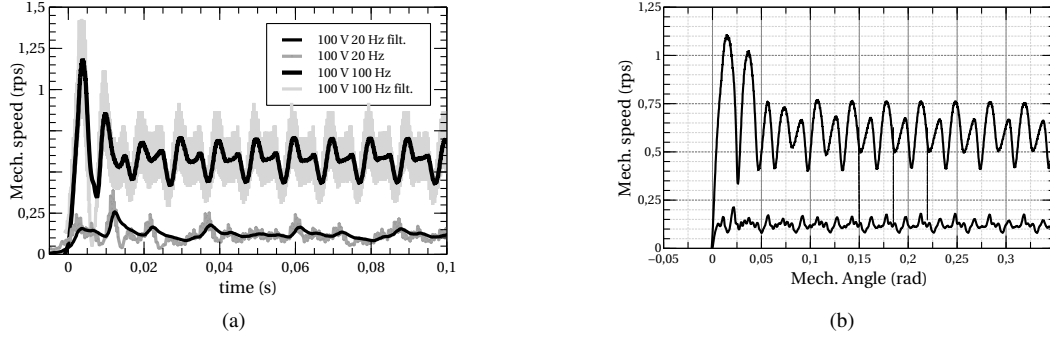
Fig. 4. Transient test for frequency step: (a) mechanical frequency vs time and (b) mechanical frequency vs position
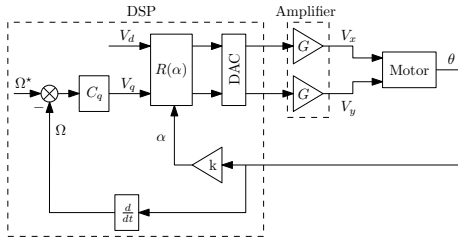


Fig. 5. Schematic of the closed loop control in the $\{d, q\}$

## C. Closed loop performances

On Fig. 6, experimental results of the closed loop are represented for a speed step of $0.56\,\mathrm{rev\,s^{-1}}$ ($100\,\mathrm{Hz}$ electric frequency). The upper graph is the measured speed which follows the reference, but for the variation due to the gearing eccentricity and the circularity error. The settling time is approximately $75\,\mathrm{ms}$ i.e slow compared to the benders dynamic in agreement with the discussion above. The periodic ripple is somewhat attenuated compared to open loop. The bottom graph on the same figure demonstrates that the voltage is effectively imposed in the $\{d, q\}$ axis and that only $V_q$ is varied to produce the torque required by the mechanical load that was applied during the test.

The purpose of the next test was a) to validate that no pull off would happen when the load exceed the motor capacity b) to study the capability of the controller in the case of saturation. The reference was set to $500\,\mathrm{Hz}$ at full load i.e a $2.5$ factor above specification. $V_d$ was set to $50\,\mathrm{V}$ to push the speed control into staturation. Indeed, in the implementation $V_q$ was limited to respect the limit voltage of the benders. The results are presented on fig. 7. The controller is indeed saturated when the load is braking but as soon as the load torque diminishes the controller recovers and maintains the expected value (top left). The angular offset is defined as $\Delta\alpha = \alpha - k\theta$. Ideally, it should remain constant, but in the case of pull-off it would drift away. On the top-left graph, it is verified that, even if the motor is braked, this never causes the loss of synchronism. Only slight variations of $\Delta\alpha$. The voltages in the $\{d, q\}$ frame are still imposed (bottom graph), although slight perturbations due to the saturation are now visible. Therefore, it can be concluded that the controller ensures that no pull-off occurs.
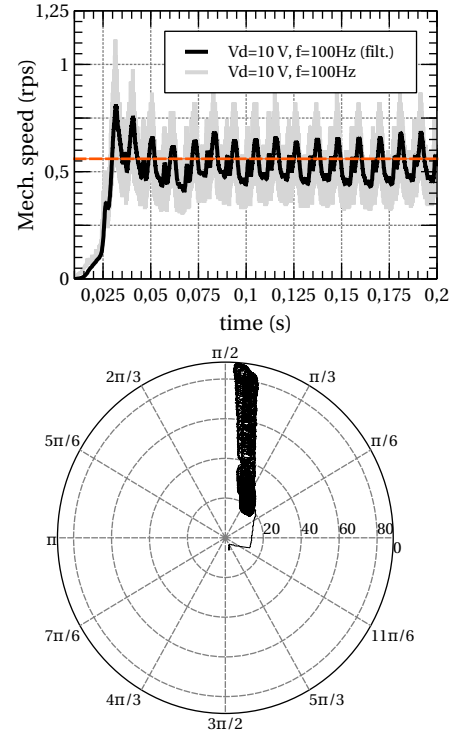


Fig. 6. Step response of the closed loop in the d,q frame: (top) mechanical instantaneaous speed vs time; (bottom) voltages in the d,q frame (resp. horizontal and vertical axis)

## V. DISCUSSION: IMPROVEMENT OVER OPEN-LOOP OPERATION

Essentially, the PAD is similar to a stepper motor, in the sense that imposing the voltage angle also imposes the shaft position thanks to the rigid kinematic constraint of the gearing: a full electric revolution results in a mechanical step of $1/178^{\mathrm{th}}$ of revolution. However, this advantage is lost if a disengagement occurs during the operation for instance in the case of excessive load torque just like step loss can occur on an overloaded stepper motor. The proposed strategy, on the other hand, guarantees that this can not happen : too large a torque may cause the motor not to follow the speed reference or even to stall as the voltage reference exceeds the supply capability, but under any circumstance the synchronization is
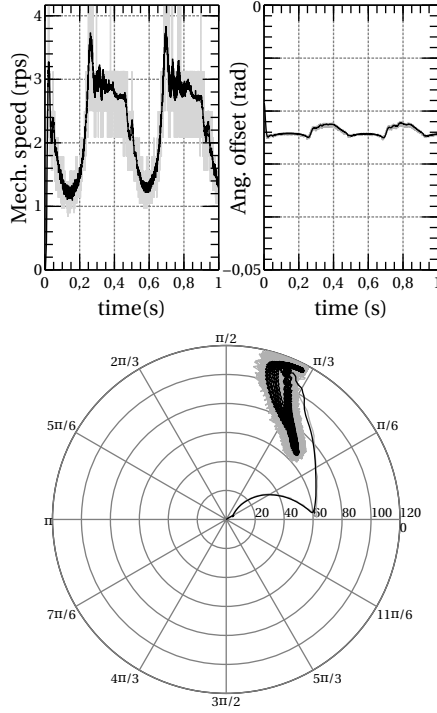
Fig. 7. Step response at full load and 500 Hz electric frequency : (up-left) mechanical instantaneous speed vs time (up-right) internal angle and (bottom) voltages in the d,q frame (resp. horizontal and vertical axis)
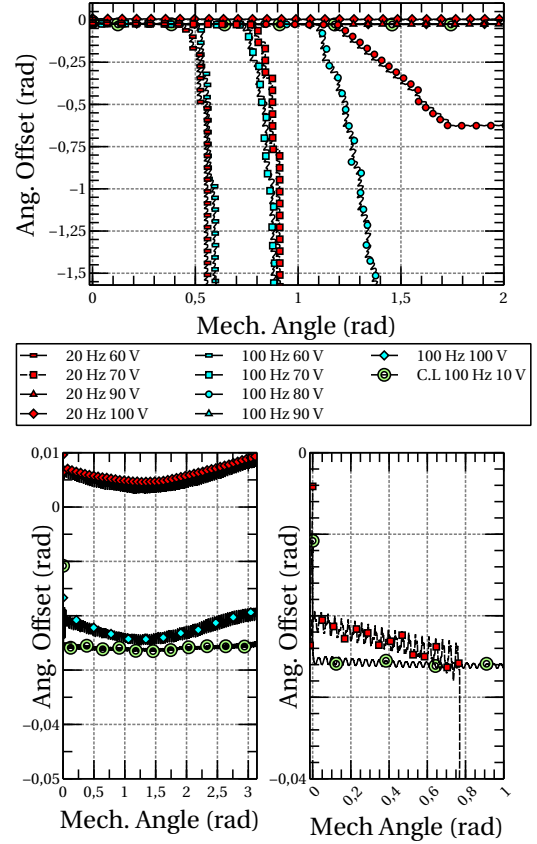


Fig. 8. Operation under loading torque for several conditions of the supply in open loop, compared to the closed loop (holed disk) : all runs (top); open loop at 100 V and closed loop (bottom left); zoom near stalling occurring during 70 V run and closed loop (bottom right)

conserved and normal operation may resume once the torque surge has disappeared.

This is illustrated on fig. 8 where the angular offset is represented as a function of the measured shaft angle. The angular offset is constant in the case of synchronicity which is the expected behaviour. The tests were performed for various voltage amplitudes (60 V to 100 V) and electric frequencies (20 Hz and 100 Hz). For comparison, the closed loop is also represented (reference frequency 100 Hz, $V_d$ =10 V).

On the top graph, the results show that for voltages lower than 90 V, the motor stalls (non horizontal branches) for various angle following roughly a linear relationship with regard to voltage while the influence of frequency is less clear (due to the low inertia). On the bottom left graph, the 100 V/20 Hz, 100 V/100 Hz and the closed loop tests are represented separately. For the open loop cases, the slip angle evolves around $8.8 \times 10^{-3}$ rad or $26.5 \times 10^{-3}$ rad that is electric angle around $\frac{\pi}{2}$ rad and $-\frac{3\pi}{2}$ rad. This is consistent with the model: the speed and the voltage being imposed, the angle varies in order to modulate the torque according to the power required. By contrast, in the case of the closed loop, the voltage is modulated according to the torque requirement by the controller, and the electric angle is almost constantly $-\frac{3\pi}{2}$ rad. Finally, the right graph of fig. 8 is a zoom near the stalling of the motor (60 V 20 Hz): the motor stops as soon as the electric angle goes below the $-\frac{3\pi}{2}$ rad limit as the torque characteristic becomes unstable similarly to a synchronous machine. On fig. 9 the voltages at 100 Hz in open and closed loop vs position (left) and in the rotating frame (right) illustrate

the effect of the implemented control on the voltages applied. While the voltages applied in open loop remain constant (and are interrupted before the end of the test if pull-off happens), the voltage in closed loop is modulated according to the torque requirements.

## VI. CONCLUSION

This paper has proposed a model that highlights the similitude between the PAD and the synchronous motors by introducing a rotating frame $\{d,q\}$ synchronized with the mechanical angle of the rotor. This gives rise to the following observations (valid for the convention of the paper which suppose that at $t = 0$ the $d$ axis is aligned with the origin of the angular position of the shaft) :

- the component in the $d$-axis of the voltage vector controls the contact force;
- the component in the $q$-axis of the voltage vector controls the torque.

A simple controller has been implemented, based on this strategy to demonstrate the improvement which are :

- during the tests the motor did not stall;
- voltages are modulated as opposed to the open loop which requires at least 90 V for the specimen under
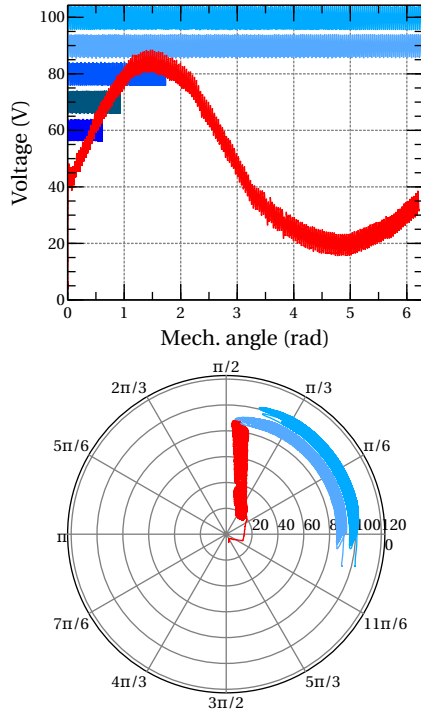
Fig. 9. Voltages applied in open and closed loop vs shaft position(left) and in the $\{d, q\}$ electric frame (right) at $100\,\text{Hz}$.

investigation, leading to lower power requirements and less self heating;

- in closed-loop and full load, run at speeds up to 168 rpm were conducted as opposed to open-loop for which the motor would not start above 67 rpm.

Despite the significant improvements that were discussed, the use of the encoder is a drawback even if it has not to be as precise as the model used in this paper. Future work will address this issue, either by a sensorless approach [20] or by implementation of integrated sensors.

## Acknowledgment

## VII. References

### References

[1] G. S. Fischer, A. Krieger, I. Iordachita, C. Csoma, L. L. Whitcomb, G. Fichtinger, MRI Compatibility of Robot Actuation Techniques – A Comparative Study, in: Medical Image Computing and Computer-Assisted Intervention – MICCAI 2008, Lecture Notes in Computer Science, Springer, Berlin, Heidelberg, 2008, pp. 509–517.

[2] Y. Koseki, N. Koyachi, T. Arai, K. Chinzei, Remote actuation mechanism for MR-compatible manipulator using leverage and parallelogram-workspace analysis, workspace control, and stiffness evaluation, in: Robotics and Automation, 2003. Proceedings. ICRA'03. IEEE International Conference on, Vol. 1, IEEE, 2003, pp. 652–657.

[3] R. Gassert, R. Moser, E. Burdet, H. Bleuler, MRI/fMRI-compatible robotic system with force feedback for interaction with human motion, IEEE/ASME Transactions on Mechatronics 11 (2) (2006) 216–224.

[4] M. Turkseven, J. Ueda, Control of Pneumatic Actuators with Long Transmission Lines for Rehabilitation in MRI, in: 2016 International Symposium on Experimental Robotics, Springer Proceedings in Advanced Robotics, Springer, Cham, 2016, pp. 84–91.

[5] V. Groenhuis, J. Veltman, F. J. Siepel, S. Stramigioli, Stormram 3: A magnetic resonance imaging-compatible robotic system for breast biopsy, IEEE Robotics Automation Magazine 24 (2) (2017) 34–41.

[6] D. Stoianovici, C. Kim, G. Srimathveeravalli, P. Sebrecht, D. Petrisor, J. Coleman, S. B. Solomon, H. Hricak, MRI-Safe Robot for Endorectal Prostate Biopsy, IEEE/ASME Transactions on Mechatronics 19 (4) (2014) 1289–1299.

[7] G. S. Fischer, I. Iordachita, C. Csoma, J. Tokuda, S. P. DiMaio, C. M. Tempany, N. Hata, G. Fichtinger, MRI-Compatible Pneumatic Robot for Transperineal Prostate Needle Placement, IEEE/ASME Transactions on Mechatronics 13 (3) (2008) 295–305.

[8] Y. Chen, K.-W. Kwok, Z. T. H. Tse, An MR-Conditional High-Torque Pneumatic Stepper Motor for MRI-Guided and Robot-Assisted Intervention, Annals of Biomedical Engineering 42 (9) (2014) 1823–1833.

[9] Y. Wang, G. A. Cole, H. Su, J. G. Pilitsis, G. S. Fischer, MRI compatibility evaluation of a piezoelectric actuator system for a neural interventional robot, in: 2009 Annual International Conference of the IEEE Engineering in Medicine and Biology Society, 2009, pp. 6072–6075.

[10] H. Su, W. Shang, G. Cole, G. Li, K. Harrington, A. Camilo, J. Tokuda, C. M. Tempany, N. Hata, G. S. Fischer, Piezoelectrically Actuated Robotic System for MRI-Guided Prostate Percutaneous Therapy, IEEE/ASME Transactions on Mechatronics 20 (4) (2015) 1920–1932.

[11] M. Turkseven, J. Ueda, Observer based impedance control of a pneumatic system with long transmission lines, in: Robotics and Automation (ICRA), 2016 IEEE International Conference on, IEEE, 2016, pp. 1160–1165.

[12] D. Stoianovici, D. Song, D. Petrisor, D. Ursu, D. Mazilu, M. Mutener, M. Schar, A. Patriciu, "MRI Stealth" robot for prostate interventions, Minimally Invasive Therapy & Allied Technologies 16 (4) (2007) 241–248.

[13] A. Abadi, G. Kosa, Piezoelectric beam for intrabody propulsion controlled by embedded sensing, IEEE/ASME Transactions on Mechatronics 21 (3) (2016) 1528–1539.

[14] P. Shokrollahi, J. M. Drake, A. A. Goldenberg, Signal-to-noise ratio evaluation of magnetic resonance images in the presence of an ultrasonic motor, BioMedical Engineering OnLine 16 (1) (2017) 1–12.

[15] T. Suzuki, H. Liao, E. Kobayashi, I. Sakuma, Ultrasonic motor driving method for EMI-free image in MR image-guided surgical robotic system, IEEE, 2007, pp. 522–527.

[16] A. Kappel, B. Gottlieb, C. Wallenhauer, Piezoelektrischer Stellantrieb (PAD) (Piezoelectric Actuator Drive (PAD)), at - Automatisierungstechnik 56 (3/2008).

[17] C. Mangeot, Operation of a quasi-static piezomotor in transitory frequency range up to resonance, in: Actuator 2014, Actuator, BREMEN, Germany, 2014, pp. 1–4.

[18] C. Giraud-Audine, M. Amberg, F. Giraud, C. Mangeot, B. Lemaire-semail, Dynamic model of a PAD actuator : dynamic operations and pull-off at high speed, in: ACTUATOR 2016, proceedings ACTUATOR 2016, BREMEN, Germany, 2016, pp. 1–4.

[19] R. Zeichfussl, B. Gottlieb, C. Wallenhauer, S. Herzig, A. Kappel, T. Luth, A method for auto-adjustment of a new piezoelectric drive, in: Mechatronics, 2009. ICM 2009. IEEE International Conference on, IEEE, 2009, pp. 1–6.

[20] M. Rakotondrabe, I. A. Ivan, S. Khadraoui, P. Lutz, N. Chaillet, Simultaneous Displacement/Force Self-Sensing in Piezoelectric Actuators and Applications to Robust Control, IEEE/ASME Transactions on Mechatronics 20 (2) (2015) 519–531.

**Dr. Christophe Giraud-Audine** (M'11) received his M.Eng. in mechanical engineering from the École Nationale Supérieure d'Arts et Métiers in 1992. From 1993 to 1995, he teached control technics, mechatronic and power electronic at the Ecole Nationale Supérieure Universitaire Technologique in Dakar, Senegal. He received his Ph.D degree in electrical engineering from the Institut National Polytechnique de Toulouse in 1998. From 1998 to 2000, he worked as a Research Associate in the Electric Machines and Drives group at the University of Sheffield. Since, he joined an associate professor position at the École Nationale Supérieure d'Arts et Métiers. He joined the L2EP in 2011, his research focuses on the modelling and control of devices based on piezoelectric actuators applied to mechanical processes, servo actuators, haptic devices and vibration control.

**Dr Frédéric Giraud** (M'04) received the B.s. degree in 1995 from Paris-XI University, graduated from the Ecole normale supérieure de cachan, France in 1996 in electrical engineering, and received the M.s. degree in electrical engineering in 1997 from the Institut national Polytechnique de Toulouse and the Ph.d. degree in electrical engineering in 2002 from the University lille 1. He is a member of the L2EP, where he works as an associate Professor. His research deals with the modeling and control of piezoelectric actuators. He is Associate Editor of IEEE Transactions on Haptics.

**Michel Amberg** Michel Amberg has been teaching electronics at the University of Lille, France. He graduated from the Ecole Normale Supérieure de Cachan in electrical engineering, France in 1981. He has tutored more than a hundred bachelor's students during their projects in the field of telecommunications, computer science, and electronics. He is now a research engineer at IRCICA, and works on the electronic design of tactile devices.

**Charles Mangeot** Charles E. Mangeot received the M.Sc. degree in manufacturing from Cranfield University, Cranfield, United Kingdom, in 2001, and the M.Eng. degree in mechanical engineering from Ecole Nationale Supérieure des Arts et Métiers, Paris, France, in 2002. From 2002 to 2006 , he was with Sagem Défense et Sécurité , Paris, working on the design and testing of electromechanical actuators for aerospace. At present, he is Senior Research and Development Engineer with Noliac, Denmark, now part of the CTS Corporation, Chicago, USA. His research has been concerned with design and modelling of piezoelectric actuators. Mr. Mangeot is a member of the European Society for Precision Engineering and Nanotechnology.

**Pr B. Lemaire-Semail** (M'87) received the BS degree from Paris XI University, Orsay, France in 1985, the graduate degree in applied physics from Ecole Normale Supérieure de Cachan, France, in 1986 and the MS degree from Universities Paris VI and Paris XI, France in 1987. She received her Ph. D degree in 1990 from University of Paris XI, and habilitation degree in 1997 from University of Science and Technology of Lille. Since 1990 she has been assistant professor in Ecole Centrale of Lille, till 1998, and she is now professor in University of Lille. Since 2015, she is the head of the electrical engineering and power electronics laboratory of Lille (L2EP). She has been studying electromagnetic motors and currently, her main field of interest deals with the modelling and control of piezo-electric actuators, for positioning and haptic applications.